Check for updates

Removal of Cr(VI) and methyl orange by activated carbon fiber supported nanoscale zero-valent iron in a continuous fixed bed column

Jian Liu, Zhengji Yi, Ziling Ou and Tianhui Yang

ABSTRACT

The application of activated carbon fiber supported nanoscale zero-valent iron (ACF-nZVI) in the continuous removal of Cr(VI) and methyl orange (MO) from aqueous solution was studied in depth. The breakthrough curves of Cr(VI) in a fixed bed with ACF-nZVI were measured, and compared with those in the fixed bed with ACF. The catalytic wet peroxide oxidation (CWPO) process for MO was also carried out using ACF-nZVI after reacting with Cr(VI) in the same fixed bed. The results showed that the breakthrough time of ACF-nZVI was significantly longer than that of ACF. Higher pH values were unfavorable for the Cr(VI) removal. The breakthrough time increased with decreasing inlet Cr(VI) concentration or increasing bed height. The Yoon–Nelson and bed depth service time (BDST) models were found to show good agreement with the experimental data. The Cr(VI) removal capacity when using ACF-nZVI was two times higher than that when using ACF. Under the optimal empty bed contact time of 1.256 min, the fixed bed displayed high MO conversion (99.2%) and chemical oxygen demand removal ratio (55.7%) with low Fe leaching concentration (<5 mg/L) after continuous running for 240 min. After three cycles, the conversion of MO remained largely unchanged.

Key words | activated carbon fiber, BDST model, Cr(VI), methyl orange, nanoscale zero-valent iron, Yoon–Nelson model

Jian Liu (corresponding author)
Zhengji Yi
Ziling Ou
Tianhui Yang
College of Chemistry and Materials Science,
Hengyang Normal University,
Hengyang 421008,
China
E-mail: *liujianzyx@163.com*

Jian Liu
Zhengji Yi
Key Laboratory of Functional Metal-Organic Compounds of Hunan Province,
Hengyang Normal University,
Hengyang 421008,
China
and
Key Laboratory of Functional Organometallic Materials,
University of Hunan Province, Hengyang Normal University,
Hengyang 421008,
China

HIGHLIGHTS

- Activated carbon fiber supported nanoscale zero-valent iron (ACF-nZVI) can be continuously used to remove Cr(VI) and methyl orange (MO).
- The Cr(VI) removal kinetics were fitted well by Yoon–Nelson and bed depth service time models.
- ACF-nZVI showed two times higher Cr(VI) removal capacity than ACF.
- The used ACF-nZVI showed an excellent degradation performance for MO.
- The conversion of MO remained basically unchanged after three cycles.

INTRODUCTION

Cr(VI) is a common toxic heavy metal ion in wastewater, which is widely used in mining, electroplating, leather tanning, pigment, etc. (Xu *et al.* 2014; Shang *et al.* 2014). Cr(VI) may exist in the aqueous solution in three different ionic forms ($HCrO_4^-$, CrO_4^{2-} or $Cr_2O_7^{2-}$), the distribution of which depends on solution pH (Kim *et al.* 2012). It is harmful to most living organisms and difficult to biodegrade. Chromium compounds have been classified as human carcinogens by the International Agency for Research on Cancer (Chen *et al.* 2018). Among various dyes, methyl orange (MO) is a typical water-soluble anionic azo dye being widely used in various industries such as dyeing, textile, paper, and leather (Subbaiah & Kim 2016; Yan *et al.* 2016). Azo dyes bring serious harm to the water environment and human health due to their dark color, high toxicity (carcinogenicity, teratogenicity, etc.), and stable complex

doi: 10.2166/wst.2020.383

Downloaded from http://iwaponline.com/wst/article-pdf/82/4/732/744832/wst082040732.pdf
by guest

aromatic molecular structure (Martínez-Huitle & Brillas 2009; Wang *et al.* 2015; Sakir & Onses 2019). Therefore, effective removal of Cr(VI) and azo dye from wastewater is a hot topic in the field of water purification.

Various physical and chemical methods have been developed to treat heavy metal ions and azo dyes. The optimization of treatment materials has always been the focus of improving the effectiveness of wastewater treatment. Nanoscale zero-valent iron (nZVI) is often used to remove contaminants from wastewater because of its strong reducibility with the redox potential of –0.44 V (Fan *et al.* 2019) and surface activity (Li *et al.* 2019). For example, the nZVI can reduce Cr(VI) to low-toxic insoluble Cr(III); meanwhile, the nZVI is oxidized to Fe(II) or Fe(III) (Dong *et al.* 2016). However, nZVI is usually aggregated because of its high surface energy and intrinsic magnetic interactions (Diao *et al.* 2016), which will lead to the decrease of specific surface area and the reduction of reactivity. Immobilization of nZVI onto supporting materials is an effective method to solve these problems (Sheng *et al.* 2016). Catalytic wet hydrogen peroxide oxidation (CWPO) is a simple and efficient oxidation process, which stimulates hydrogen peroxide to produce hydroxyl radicals and then degrade azo dyes using transition metals (such as Fe(II) or Fe(III)) as catalyst (Fenton-like reactions) (Ramirez *et al.* 2007; Herney-Ramireza *et al.* 2011). However, it also has some drawbacks, such as difficult recovery of catalyst, easy leaching of metal ions and low reusability (Neamţu *et al.* 2004; Quintanilla *et al.* 2007; Yan *et al.* 2014). To overcome these disadvantages, developing heterogeneous catalysts (namely, transition metal supported on porous materials) has attracted more and more attention in recent years. Activated carbon fiber (ACF) is often used as an adsorbent or catalyst support for the removal of heavy metals and azo dyes because of its developed surface area, large adsorption capacity and high adsorption/desorption rate (Zhang *et al.* 2015; Carraro *et al.* 2019; Liu *et al.* 2019).

Effective combination of nZVI and ACF not only makes use of the high adsorption capacity of ACF and high reduction capacity of nZVI, but also overcomes the disadvantage of aggregation of nZVI. The immobilization of the nZVI on ACF has been used to remove Cr(VI). Huang *et al.* (2014) investigated the removal performance of activated carbon fiber felt (ACFF), nZVI and ACFF-nZVI by batch experiments, and the results showed the removal ratio of Cr(VI) was 67.0% for ACFF-nZVI, which was higher than that for ACFF (52.6%) and nZVI (59.4%). Qu *et al.* (2017) studied the removal of Cr(VI) from groundwater using ACF-nZVI composite in a permeable reactive column, and the results showed that ACF-nZVI still kept a Cr(VI) removal rate of more than 90% after five cycles. However, according to the literature, most of the studies were carried out in batch reactors, and there were few reports in a continuous fixed bed reactor. Moreover, according to the mechanism that nZVI can be oxidized to Fe(II) or Fe(III) (Fenton-like catalyst) by Cr(VI), there is no literature on CWPO of MO using ACF-nZVI after reacting with Cr(VI). The objective of this work is to investigate the removal performance of Cr(VI) in a continuous fixed bed with ACF-nZVI and the degradation effect of MO in the same fixed bed. The removal kinetics of Cr(VI) are examined by both Yoon–Nelson and bed depth service time (BDST) models.

EXPERIMENTAL

Materials

Activated carbon fiber felts were purchased from Jiangsu Tongkang Special Activated Carbon Fiber & Fabric Co., Ltd in China and cut into small circles (2 cm diameter). All of the chemicals used were analytical grade.

Preparation of ACF-nZVI

Activated carbon fiber supported nanoscale zero-valent iron (ACF-nZVI) was prepared using ACF as carrier and $NaBH_4$ as reducing agent by liquid phase reduction method (Sun *et al.* 2006; Zhang *et al.* 2010; Huang *et al.* 2014). Briefly, ACF was added to ferrous sulfate heptahydrate solution (0.1 mol/L, $V_{ethanol}:V_{water} = 1:4$) and soaked for 0.5 h ($m_{Fe}:m_{ACF} = 0.25:1$). Then an equal volume of freshly prepared $NaBH_4$ water solution (0.5 mol/L) was slowly dripped into the mixed solution of ACF and Fe^{2+}. After 2 h, the samples were filtered and washed twice with absolute ethanol, then dried in a vacuum oven. The reduction reaction is as follows (Xu *et al.* 2014):

$$Fe^{2+} + 2BH_4^- + 6H_2O \rightarrow Fe^0 + 2B(OH)_3 + 7H_2 \uparrow \quad (1)$$

Characterization of ACF-nZVI

The morphology of ACF and ACF-nZVI samples was characterized by a scanning electron microscope (SEM, Zeiss EVO10, Germany).

The composition of the ACF-nZVI was determined by X-ray diffraction (XRD, Bruker D8 Advance, Germany)

Downloaded from http://iwaponline.com/wst/article-pdf/82/4/732/744832/wst082040732.pdf
by guest

using Cu Ka irradiation at 40 kV and 40 mA with 2θ range from 5° to 90°.

The valence state of iron on the surface of the ACF-nZVI was analyzed by an X-ray photoelectron spectrometer (XPS, Thermo Escalab 250Xi, USA) using an Al Ka radiation source.

Cr(VI) removal kinetics experiments

Kinetics experiments of Cr(VI) removal were conducted in a continuous fixed bed made of a stainless steel tube (inner diameter = 2 cm, length = 8 cm) at 30 °C and atmospheric pressure.

To obtain a uniform distribution of the inlet Cr(VI) solution inside the fixed bed and ensure the desired temperature, the stainless steel tube was filled with inert glass beads (diameter = 2–3 mm) at both ends and ACF-nZVI (or ACF) in the middle. Cr(VI) solution was carried to the stainless steel reactor by a BT101 L peristaltic pump in up-flow mode, and temperature of the reactor was controlled by a water bath (Figure 1). In the feed tank, the pH of Cr(VI) solution was adjusted with nitric acid. The effects of initial pH value of Cr(VI) solution (2, 3 and 4), bed height (0.8, 1.2 and 1.6 cm) and inlet Cr(VI) concentration (100, 200 and 300 mg/L) on the removal of Cr(VI) were studied. The feed flow rate was fixed at 2 mL/min. The absorbance at the inlet and outlet of the solution was determined by 1,5-diphenylcarbazide spectrophotometry (GB7467-87 1987) at 540 nm using a V5100 visible spectrophotometer. The experimental results are shown in the form of breakthrough curves, i.e., the variations of C/C_0 (outlet concentration/inlet concentration) versus time.

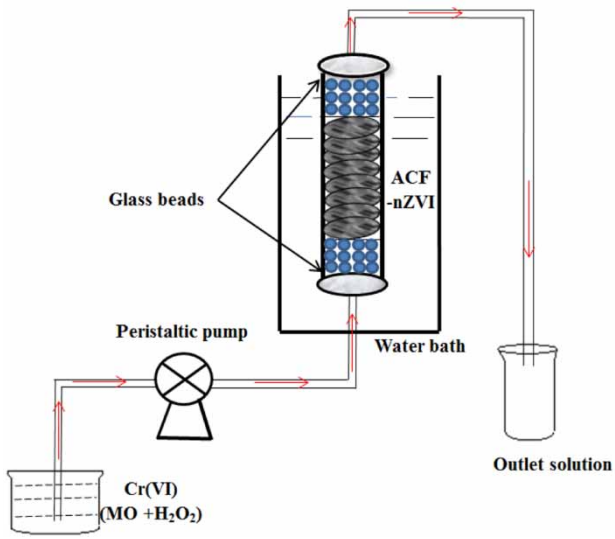

Figure 1 | Flow diagram of the fixed bed experimental column.

MO degradation experiments

The MO degradation experiments were carried out in the same fixed bed reactor using ACF-nZVI after reacting with Cr(VI) solution (Figure 1). In the feed tank, the MO solution (50 mg/L) and hydrogen peroxide (17.6 mM) were mixed uniformly after pH was adjusted to 2 by nitric acid. The reactor was heated by a hot water bath to maintain 70 °C at atmospheric pressure. The effects of empty bed contact time (EBCT) on the removal of MO were studied. The catalysts were reused three times to examine their stability. The concentration of inlet and outlet MO solution was measured by using a V5100 visible spectrophotometer at 464 nm. The MO conversion ratio (X_{MO}, %) was calculated as follows:

$$X_{MO}(\%) = \left(\frac{C_0 - C}{C_0}\right) \times 100\% \quad (2)$$

where C_0 (mg/L) is the inlet MO concentration and C (mg/L) is the outlet concentration of MO solution at instant time t (min).

Chemical oxygen demand (COD) concentration of the outlet solution was tested by dichromate method (GB11914-89 1989). And COD removal ratio (X_{COD}, %) was calculated as follows:

$$X_{COD}(\%) = \frac{[COD]_0 - [COD]_t}{[COD]_0} \times 100\% \quad (3)$$

where $[COD]_0$ (mg/L) is the inlet COD value and $[COD]_t$ (mg/L) is the outlet COD value at time t (min).

Iron leaching concentration (mg/L) in the outlet solution was measured by using a TAS-990AFG atomic absorption spectrophotometer.

RESULTS AND DISCUSSION

Characterization of the composites

Heterogeneous surface morphology plays an important role in particle adsorption (Cui *et al.* 2017; Fang *et al.* 2017). The morphology of ACF and ACF-nZVI samples was observed by SEM, and the images are shown in Figure 2(a). It can be seen that the SEM image of ACF was obviously different from that of ACF-nZVI. The surface of ACF was smooth, but the surface of ACF-nZVI became rough and nZVI particles were well distributed on the surface of ACF.

Downloaded from http://iwaponline.com/wst/article-pdf/82/4/732/744832/wst082040732.pdf
by guest

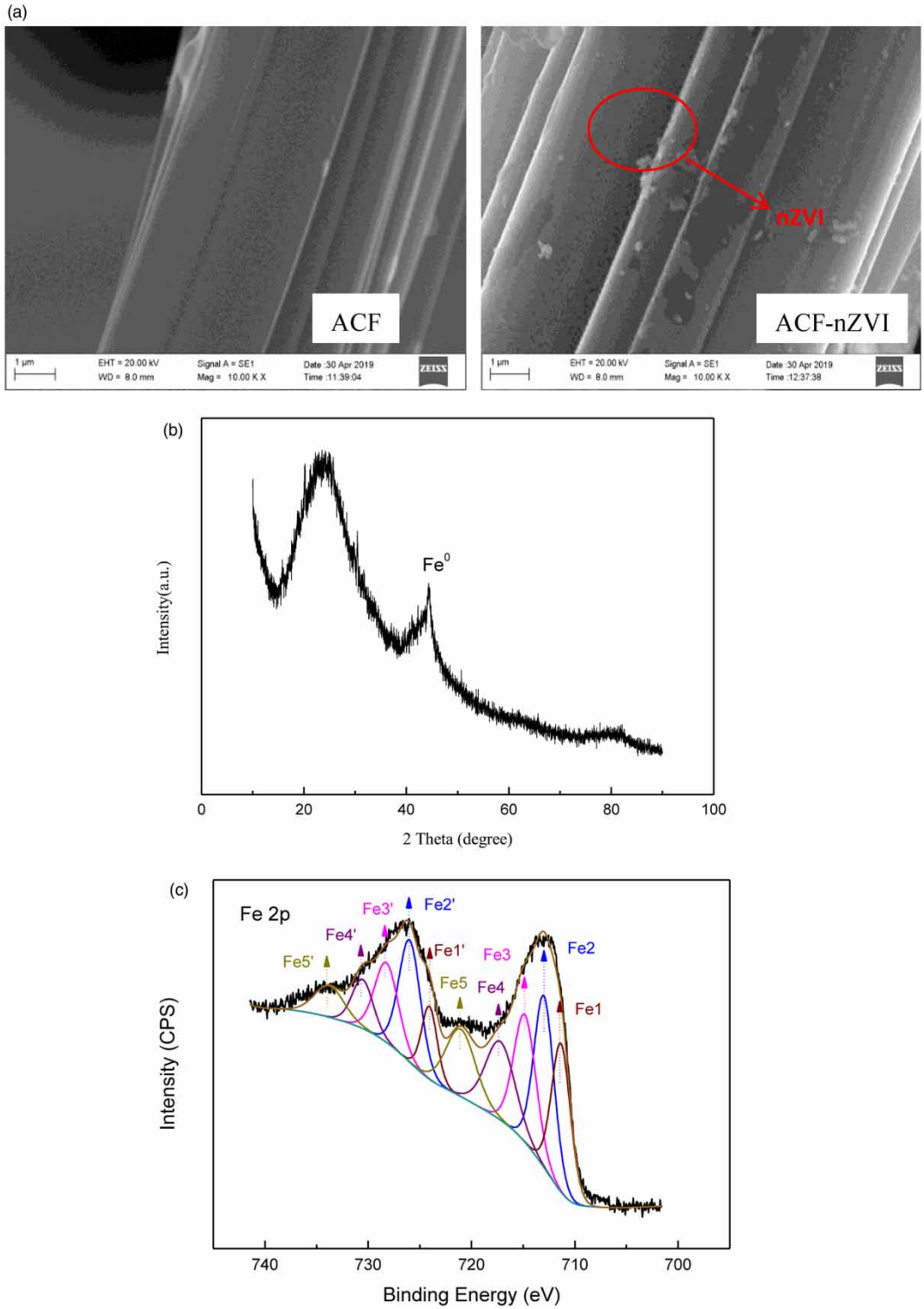

Figure 2 | Characterization of composite: (a) SEM images, (b) XRD pattern, (c) XPS pattern.

The component of ACF-nZVI was analyzed by XRD and the result is shown in Figure 2(b). The XRD patterns showed an apparent characteristic peak of carbon at 2θ of 25°, which suggested that the supports were ACFs. The diffraction peak observed at 2θ of 44.5° could be attributed to the existence of zero-valent iron. It indicates that the nZVI

Downloaded from http://iwaponline.com/wst/article-pdf/82/4/732/744832/wst082040732.pdf
by guest

particles were successfully supported by the ACFs (Huang *et al.* 2014; Liu *et al.* 2014; Zhang *et al.* 2019).

The valence state of iron on the surface of the ACF-nZVI was analyzed by XPS and the result is shown in Figure 2(c). There was no obvious characteristic peak of Fe^0, and the characteristic photoelectron peaks at 711.2, 712.59, 714.5, 716.95 and 720.44 eV (Fe1–Fe5) corresponded to the binding energies of Fe $2p_{3/2}$, while 724.07, 725.99, 728.23, 730.54 and 733.78 eV (Fe1′–Fe5′) represented the binding energies of Fe $2p_{1/2}$, which suggests the existence of different iron oxide species such as Fe^{2+} and Fe^{3+} (Fu *et al.* 2015). Combined with XRD analysis, these results show that the core of the nZVI loaded on the ACF is Fe^0, and a layer of iron oxides definitely exists on the surface of the Fe^0. Liu *et al.* (2014) prepared graphene supported nZVI, and the XPS results showed that oxidation of iron occurred all over the surface of nZVI and little Fe^0 was left. Similarly, a very weak shoulder peak corresponding to the $2p_{3/2}$ binding energy of Fe^0 was barely observable due to the high surface sensitivity of XPS (less than 10 nm in depth) for the kaolinite supported nZVI prepared by Zhang *et al.* (2011).

Kinetics of Cr(VI) removal

Effect of inlet pH value

The kinetics experiments of Cr(VI) removal were conducted in a continuous fixed bed reactor at different inlet pH values (2, 3, 4) with the Cr(VI) concentration of 100 mg/L, bed height of 1.6 cm and feed flow rate of 2 mL/min. The fixed bed was filled with ACF or ACF-nZVI. The performance of ACF and ACF-nZVI was measured by a previous set of experiments, and the results are shown in Figure 3. As can be seen from Figure 3, the breakthrough time of ACF-nZVI was significantly longer than that of ACF at each pH level under the same conditions. The breakthrough concentration reached 6.9% of the inlet concentration at 150 min for ACF, and the breakthrough concentration reached only 5.5% of the inlet concentration at 250 min for ACF-nZVI at pH 2. The breakthrough time of Cr(VI) was prolonged by loading nZVI on ACF. In addition, the breakthrough time of Cr(VI) significantly decreased with the increase of pH for both ACF and ACF-nZVI. Thus, pH plays an important role in adsorption of ACF and reduction of nZVI. As we all know, the dominant form of Cr(VI) is $HCrO_4^-$ at pH 2, and Cr(VI) mainly exists in the form of CrO_4^{2-} or $Cr_2O_7^{2-}$ at higher pH (Nethaji & Sivasamy 2014). Because the surface of ACF is positively charged at lower pH, there is a strong electrostatic attraction between the positively charged ACF surface and the negatively charged $HCrO_4^-$, which is favorable for Cr(VI) adsorption (Rangabhashiyam & Selvaraju 2015). For ACF-nZVI, besides adsorption, Cr(VI) will react with nZVI, generating Cr(III) (Equations (4)–(6)) (Fu *et al.* 2013; Huang *et al.* 2014; Dai *et al.* 2016), and Fe^{2+} or Fe^{3+} is undoubtedly yielded (Equations (7) and (8)) (Zhou *et al.* 2015). According to Equations (4)–(8), a large amount of H^+ is consumed to reduce Cr(VI). In addition, higher pH is beneficial to the deposition of Cr(III) and Fe(III) hydroxides on the nZVI surface, which inhibits further decomposition of surface iron, and leads to a decrease in the reduction efficiency of nZVI (Shi *et al.* 2011; Fu *et al.* 2013). Fu *et al.* (2013) synthesized resin supported nZVI and studied the effects of initial pH values on Cr(VI) removal by batch experiments, and the results showed that the final pH values were 7.2, 9.0, 9.1 and 9.6 at initial pH values of 3.0, 5.0, 7.0 and 9.0, respectively. Hydrogen ions consumption leads to the increase of pH value of the solution after reaction; thus an acid environment is more favorable for Cr(VI) reduction. Wu *et al.* (2013) reported that the removal rate of Cr(VI) decreased from 99.85% to 54.88% with the increase of solution pH from 2 to 11. Dong *et al.* (2017) also reported that the Cr(VI) removal was significantly reduced with increasing solution pH value.

$$Cr_2O_7^{2-} + 14H^+ + 6e^- \rightarrow 2Cr^{3+} + 7H_2O \quad (4)$$

$$CrO_4^{2-} + 8H^+ + 3e^- \rightarrow Cr^{3+} + 4H_2O \quad (5)$$

$$HCrO_4^- + 7H^+ + 3e^- \rightarrow Cr^{3+} + 4H_2O \quad (6)$$

$$3Fe^0 + 2HCrO_4^- + 14H^+ \rightarrow 2Cr^{3+}3Fe^{2+} + 8H_2O \quad (7)$$

$$3Fe^{2+} + HCrO_4^- + 7H^+ \rightarrow Cr^{3+} + 3Fe^{3+} + 4H_2O \quad (8)$$

Effect of bed height

To study the effect of bed height on the removal performance of Cr(VI), the breakthrough curves of Cr(VI) in the fixed bed with different bed heights (0.8, 1.2, 1.6 cm) were measured at a constant flow rate of 2 mL/min, pH 2 and inlet concentration of 100 mg/L. The results are presented in Figure 4(a). It can be seen that the breakthrough curves at different bed heights showed the same characteristic shapes, but the Cr(VI) breakthrough time was prolonged with the increase of bed height. When the bed height was 0.8, 1.2 and 1.6 cm, the

Downloaded from http://iwaponline.com/wst/article-pdf/82/4/732/744832/wst082040732.pdf
by guest

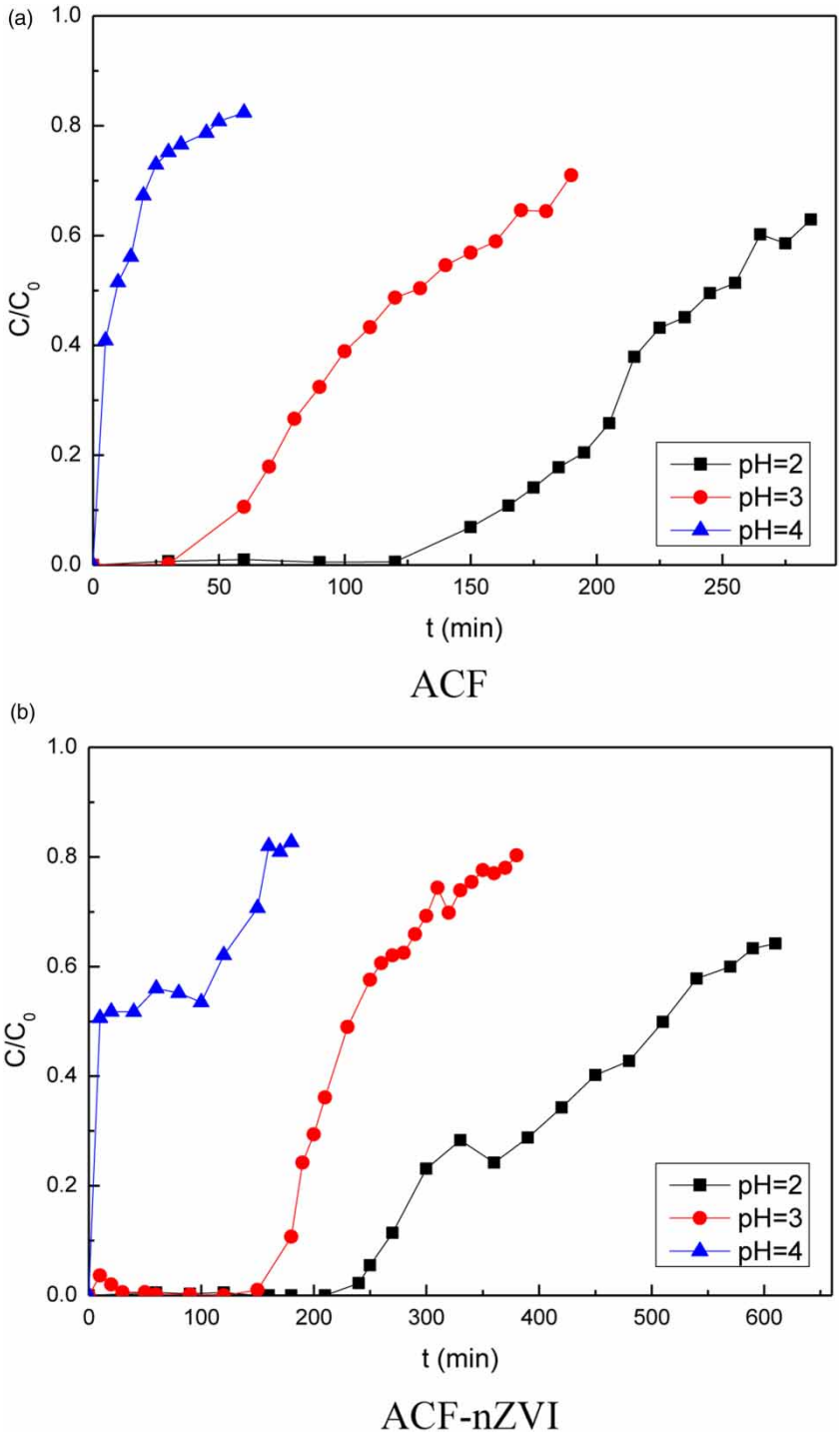

Figure 3 | Breakthrough curves for Cr(VI) removal at different pH values.

breakthrough concentration reached 2.7%, 2.6% and 5.5% of the inlet concentration at 60, 120, and 250 minutes, respectively. This could be attributed to the fact that the active sites (adsorption and reduction sites) increase with increasing bed height (Chatterjee *et al.* 2018), i.e., Cr(VI) has more opportunities to be adsorbed by ACF and reacted with nZVI. Therefore, increasing bed height usually results in an increase in breakthrough time.

Downloaded from http://iwaponline.com/wst/article-pdf/82/4/732/744832/wst082040732.pdf
by guest

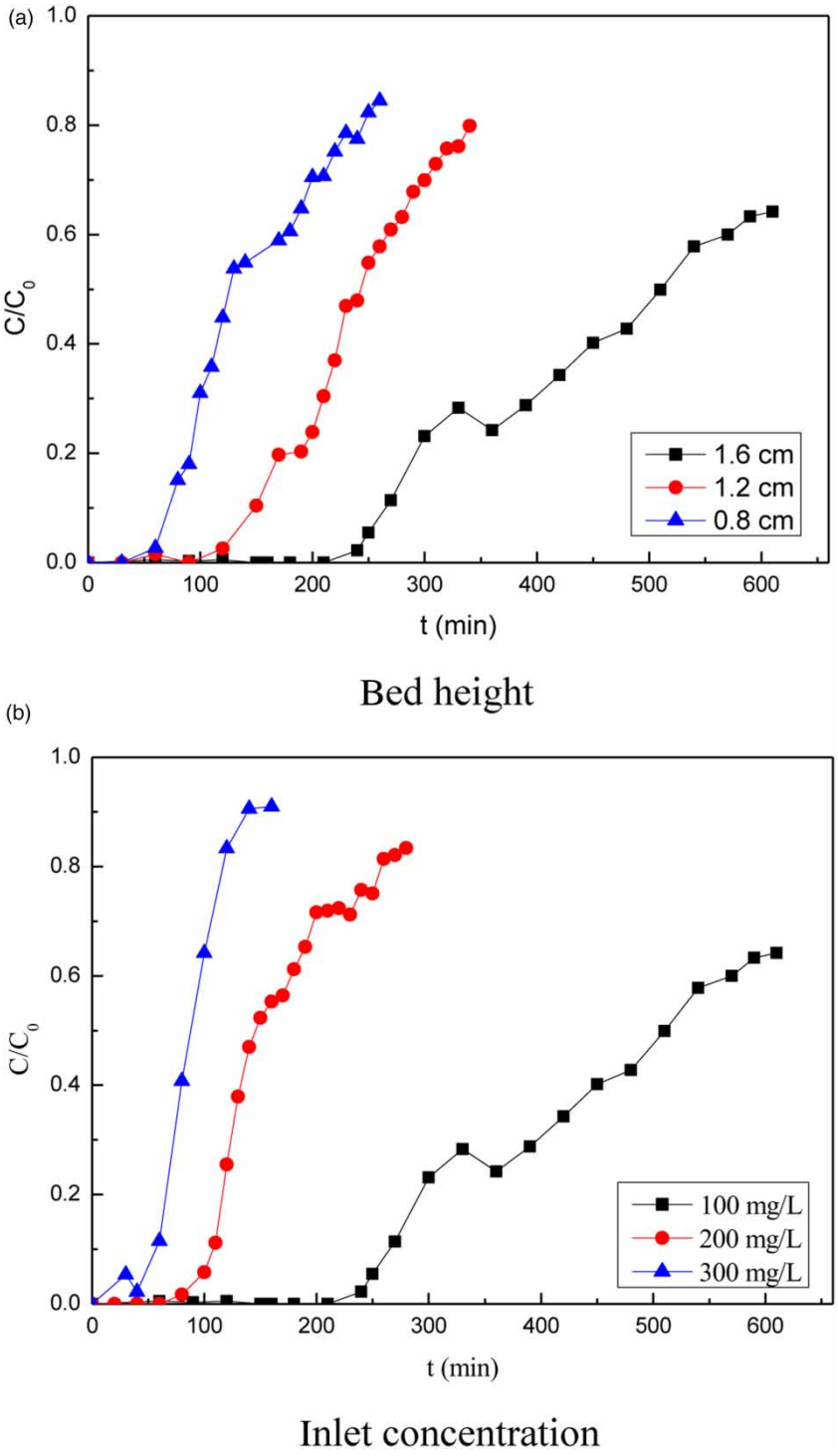

Figure 4 | Breakthrough curves for Cr(VI) removal at different bed heights and inlet concentrations.

Effect of inlet concentration

The World Health Organization recommends the maximum allowable discharge concentration of Cr(VI) into drinking water is 0.05 ppm; however, its concentration in industrial wastewater usually ranges from 5 to 220 mg/L (Ghosh 2009; Mohamed *et al.* 2016). To investigate the effect of inlet concentration on the removal performance of Cr(VI),

Downloaded from http://iwaponline.com/wst/article-pdf/82/4/732/744832/wst082040732.pdf
by guest

the breakthrough curves of Cr(VI) in the fixed bed were measured at different inlet concentrations (100, 200 and 300 mg/L), at a constant flow rate of 2 mL/min, pH 2 and bed height of 1.6 cm. The results are shown in Figure 4(b). As was evident from Figure 4(b), the breakthrough time of Cr(VI) decreased with increase in inlet concentration. When the inlet concentration was 100, 200 and 300 mg/L, the breakthrough concentration reached 11.4%, 11.2% and 11.5% of the inlet concentration at 270, 110, and 60 minutes, respectively. With the increase of inlet concentration, the treated Cr(VI) amount per unit time increases. However, the total number of binding sites available at the same bed height is constant, which may be inadequate at higher inlet concentration (Mishra *et al.* 2016; Basu *et al.* 2019). Thus, a faster adsorption saturation of ACF-nZVI in the fixed bed occurred and the breakthrough time was shortened with increasing inlet concentration. Vilvanathan & Shanthakumar (2017) studied continuous adsorption behavior of cobalt ions onto *Chrysanthemum indicum* in fixed bed columns, and the results showed early breakthrough and quick saturation were achieved at higher ion concentration. Fan *et al.* (2019) reported that higher initial Cr(VI) concentration led to faster breakthrough of the fixed bed filled with nZVI-biochar adsorbent.

Application of the Yoon–Nelson model

A simple theoretical model proposed by Yoon–Nelson was used to analyze the breakthrough curves of Cr(VI) in the fixed bed. The linear fitting of breakthrough curves in the C/C_0 region above 0.05 was performed according to Equation (9). The values of τ and k_{YN} were obtained from the intercept and slope of the time (t) versus $\ln[C/(C_0 - C)]$ plot (Figure 5). The values of these parameters and the determination coefficients (R^2) are presented in Table 1.

$$t = \tau + \frac{1}{k_{YN}} \ln \frac{C}{C_0 - C} \tag{9}$$

where t is the breakthrough time (min), k_{YN} is the rate constant (min^{-1}), τ is the time required for 50% Cr(VI) breakthrough (min), C_0 is the inlet Cr(VI) concentration (mg/L), and C is the outlet Cr(VI) concentration (mg/L).

As shown in Figure 5 and Table 1, the experimental data fitted well to the Yoon–Nelson equation, with $R^2 > 0.8$. The k_{YN} values increased with increasing inlet concentration from 100 to 300 mg/L. This may be attributed to an increase in mass transfer coefficients between Cr(VI) solution and ACF-nZVI under higher concentration gradients, and thus the adsorption and reduction rate increases. The adsorbed or reduced Cr(VI) amount per unit time increases with increasing inlet concentration, leading to an earlier breakthrough and saturation. This further explains that the breakthrough time decreased with the increase of inlet concentration. The 50% breakthrough time (τ) increased with decreasing pH or inlet concentration. With decreasing bed height, the τ value decreased. Chen *et al.* (2012) reported similar fitting results in their literature. The data in Table 1 also show that τ values fitted by the Yoon–Nelson model were close to the experimental data (Figures 3 and 4), suggesting that the Yoon–Nelson model could predict the 50% breakthrough time of Cr(VI) at different pHs, bed heights and initial concentrations without requiring further experiments.

Application of the BDST model

The BDST model was derived from the Adams–Bohart equation, but was improved by Hutchins (1973), which was used to compare the adsorption capacity of the fixed columns with different process parameters (Afroze & Sen 2016). The equation is expressed as follows:

$$t = \frac{N_0 Z}{C_0 u} - \frac{1}{k_{AB} C_0} \ln\left(\frac{C_0}{C} - 1\right) \tag{10}$$

where t is time (min), N_0 is the adsorption capacity (mg/L), Z is the bed height (cm), u is the linear velocity of Cr(VI) solution (cm/min), k_{AB} is the rate constant (L/(mg·min)), C_0 is the inlet Cr(VI) concentration (mg/L), and C is the outlet Cr(VI) concentration (mg/L) (Dissanayake *et al.* 2016).

The linear regression analysis of breakthrough curves in the C/C_0 region above 0.05 was carried out by Equation (10). The values of k_{AB} and N_0 were obtained from the slope and intercept of the time (t) versus $\ln[(C_0/C) - 1]$ plot (Figure 6). These parameter values and the R^2 values are presented in Table 2. For both the ACF and ACF-nZVI at a constant pH 2, the removal capacities (N_0) were 9.9 and 20.1 g/L, respectively. ACF-nZVI showed a Cr(VI) removal capacity two times higher than that of ACF. The values of N_0 increased with decreasing pH and initial Cr(VI) concentration but decreased with decreasing bed height. In addition, the BDST model could predict the breakthrough time (Chatterjee *et al.* 2018; Du *et al.* 2018). For example, for ACF-nZVI at pH 2, bed height of 1.6 cm

Downloaded from http://iwaponline.com/wst/article-pdf/82/4/732/744832/wst082040732.pdf
by guest

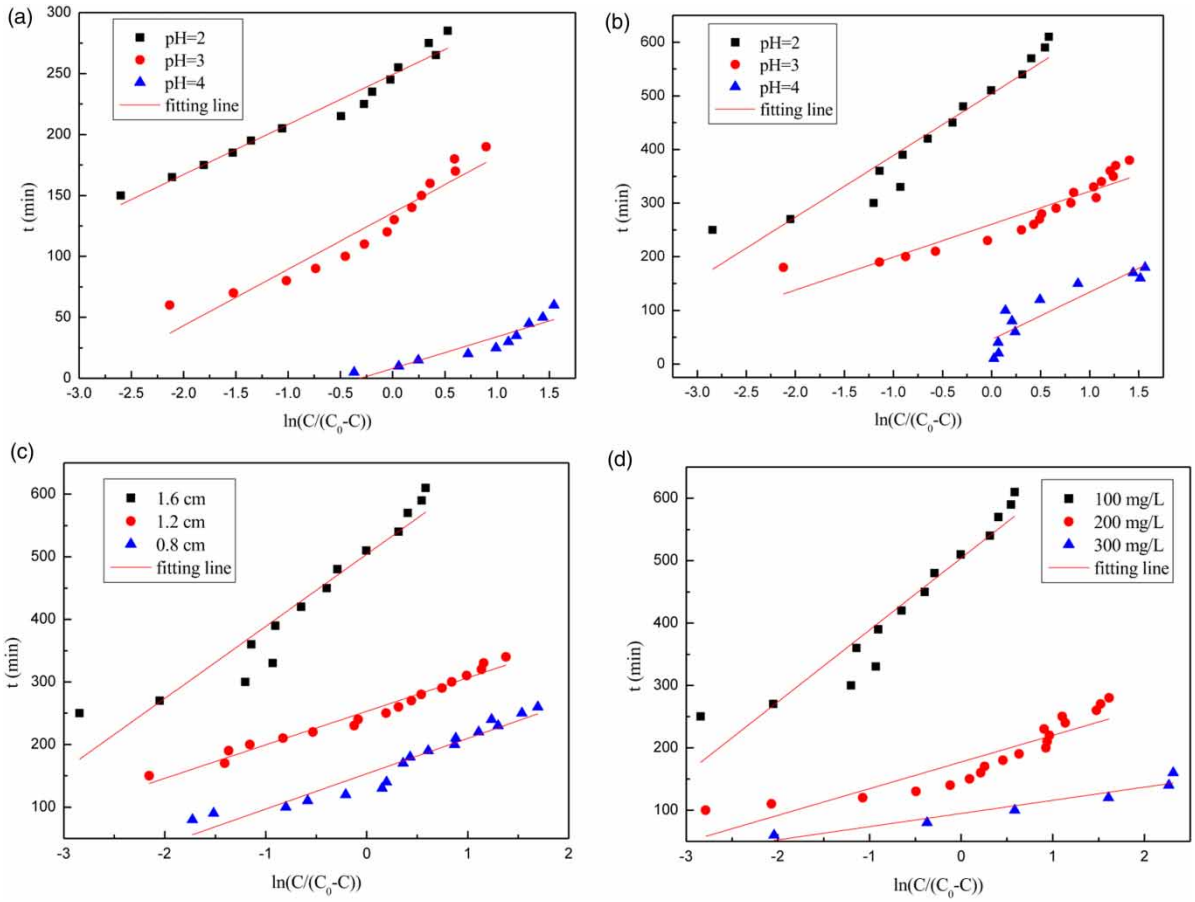

Figure 5 | Fitting plots of Yoon–Nelson model for Cr(VI) removal under different conditions: (a) ACF at different pHs, (b) ACF-nZVI at different pHs, (c) ACF-nZVI at different bed heights, (d) ACF-nZVI at different inlet concentrations.

and inlet concentration of 100 mg/L, the predicted and experimental breakthrough time for 11.4% breakthrough was 268 and 270 min, respectively.

Table 1 | Parameters of Yoon–Nelson model for Cr(VI) removal under different conditions

Materials	Bed height (cm)	pH	C_0 (mg/L)	k_{YN} (min^{-1})	τ (min)	R^2
ACF	1.6	2	100	0.0244	249	0.9618
ACF	1.6	3	100	0.0216	136	0.9074
ACF	1.6	4	100	0.0384	8	0.8466
ACF-nZVI	1.6	2	100	0.0087	504	0.9025
ACF-nZVI	1.6	3	100	0.0163	261	0.8616
ACF-nZVI	1.6	4	100	0.0113	45	0.8033
ACF-nZVI	1.2	2	100	0.0187	253	0.9695
ACF-nZVI	0.8	2	100	0.0177	153	0.9255
ACF-nZVI	1.6	2	200	0.0234	177	0.8102
ACF-nZVI	1.6	2	300	0.0474	95	0.9075

Catalytic wet peroxide oxidation of MO

Effect of EBCT

EBCT is an important parameter to measure catalyst activity and can be calculated according to the formula of catalysts volume/feed flow rate of MO. The CWPO of MO solution was carried out in a continuous fixed bed reactor at different EBCT (2.512, 1.256 and 0.628 min). The conversion ratio of MO was determined and is shown in Figure 7. It can be seen from Figure 7 that the conversion ratio of MO largely remained unchanged with the decrease of EBCT from 2.512 to 1.256 min, and the conversion ratio of MO decreased rapidly and fluctuated greatly with the further decrease of EBCT to 0.628 min. When the EBCT was 2.512, 1.256 and 0.628 min, the conversion ratio of MO was 100%, 99.2% and 33.9% respectively after the fixed bed was continuously operated for 240 min. This phenomenon can be explained by the inadequate residence time of

Downloaded from http://iwaponline.com/wst/article-pdf/82/4/732/744832/wst082040732.pdf
by guest

Table 2 | Parameters of BDST model for Cr(VI) removal under different conditions

Materials	Bed height (cm)	pH	C_0 (mg/L)	K_{AB} (mL/(mg·min))	N_0 (g/L)	R^2
ACF	1.6	2	100	0.244	9.9	0.9618
ACF	1.6	3	100	0.216	5.4	0.9074
ACF	1.6	4	100	0.384	0.3	0.8466
ACF-nZVI	1.6	2	100	0.087	20.1	0.9025
ACF-nZVI	1.6	3	100	0.163	10.4	0.8616
ACF-nZVI	1.6	4	100	0.113	1.8	0.8033
ACF-nZVI	1.2	2	100	0.187	13.4	0.9695
ACF-nZVI	0.8	2	100	0.177	12.2	0.9255
ACF-nZVI	1.6	2	200	0.117	14.1	0.8102
ACF-nZVI	1.6	2	300	0.158	11.3	0.9075

MO and H_2O_2 in the fixed bed (Albayati *et al.* 2016). Therefore, the contact time between hydrogen peroxide and iron ion is insufficient to produce enough hydroxyl radicals, and hydroxyl radicals do not have enough time to deoxidize MO according to Equations (11)–(13) (Ramirez *et al.* 2007; Herney-Ramireza *et al.* 2011), where X represents ACF.

$$\text{X-Fe(III)} + H_2O_2 \rightarrow \text{X-Fe(II)} + HO_2^{\bullet} + H^+ \quad (11)$$

$$\text{X-Fe(II)} + H_2O_2 \rightarrow \text{X-Fe(III)} + OH^- + HO^{\bullet} \quad (12)$$

$$\text{Azo dyes} + HO^{\bullet} \rightarrow \text{Products} \quad (13)$$

Stability test

To study the stability and reusability of the ACF-nZVI catalysts, three cycle experiments were carried out in the same fixed bed reactor with the EBCT of 1.256 min. After each experiment, the catalysts were recovered, washed and dried in the oven. It can be seen from Figure 8(a) that the conversion ratio of MO remained largely unchanged after three times of reuse. When the catalysts were used for the first time, the second time and the third time, the conversion ratio of MO was 99.2%, 98.3% and 99.2% respectively after

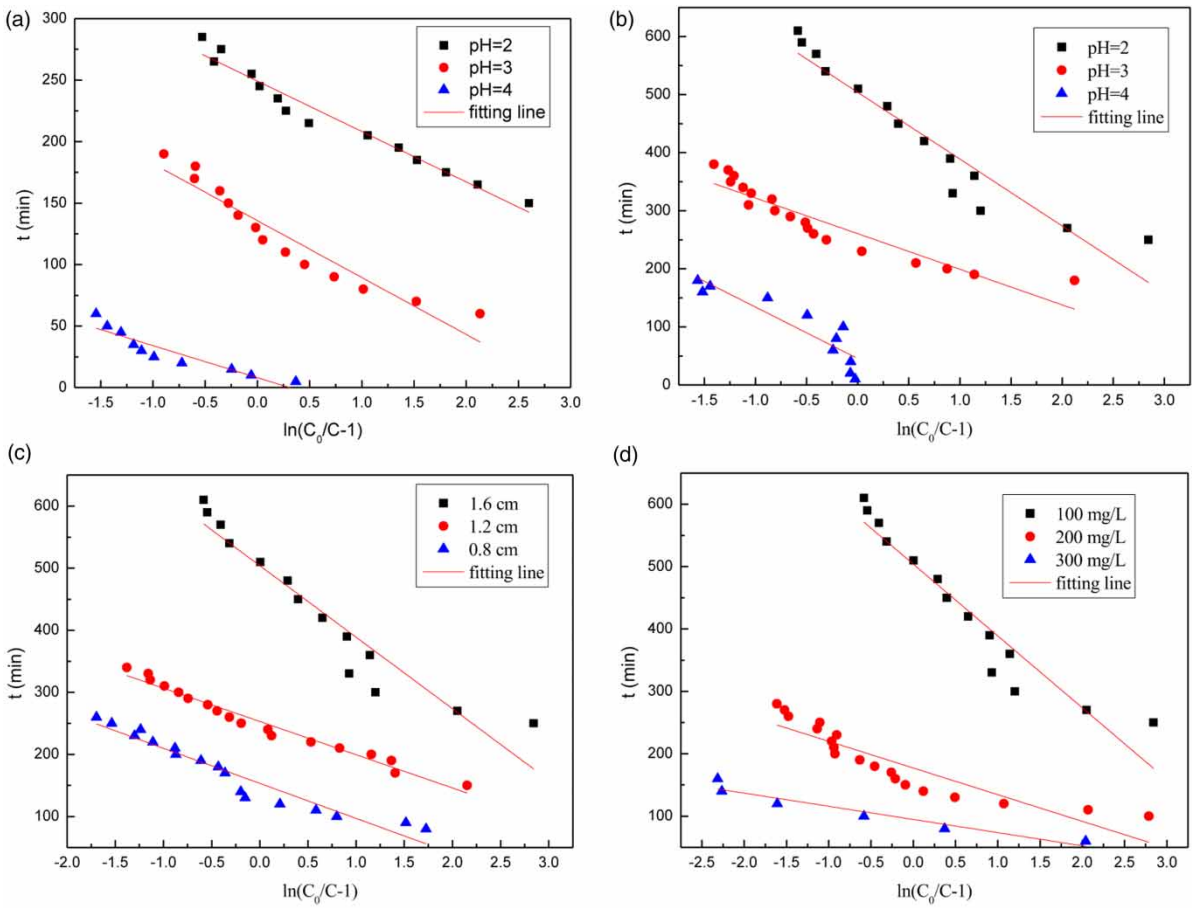

Figure 6 | Fitting plots of BDST model for Cr(VI) removal under different conditions: (a) ACF at different pHs, (b) ACF-nZVI at different pHs, (c) ACF-nZVI at different bed heights, (d) ACF-nZVI at different inlet concentrations.

Downloaded from http://iwaponline.com/wst/article-pdf/82/4/732/744832/wst082040732.pdf
by guest

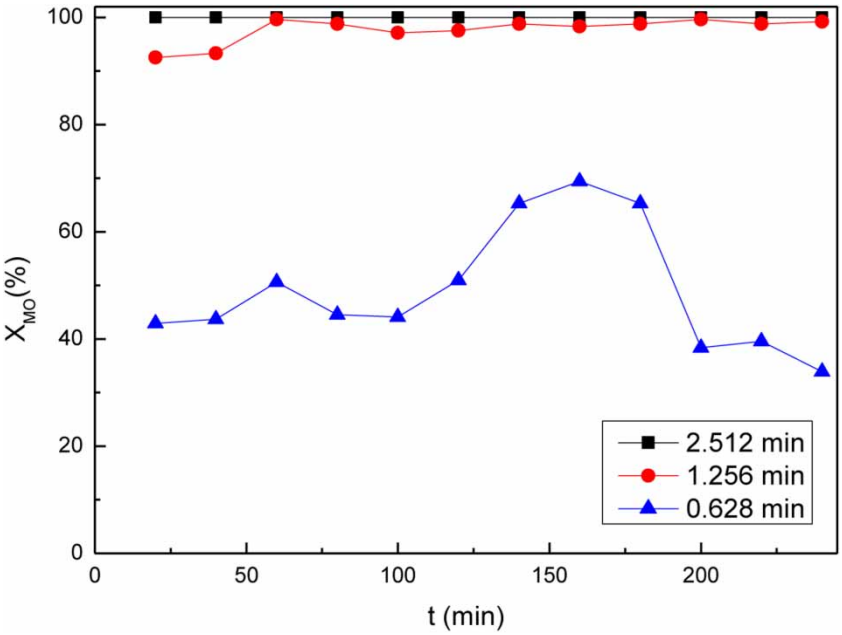

Figure 7 | Effect of EBCT on the MO degradation.

240 min of continuous operation of the fixed bed. From Figure 8(b), it can be found that the iron leaching concentration in the outlet solution fluctuated after the catalysts were reused three times, but the maximum iron leaching concentration was lower than 5.2 mg/L (<5 mg/L after first use). After three cycles, the conversion ratio of COD decreased from 55.7% to 45.3%. Iron leaching is an important factor affecting the deactivation of Fenton-like catalysts (Luca *et al.* 2018). Hence, low iron leaching concentration leads to high catalyst stability.

Adsorption of MO onto ACFs

In order to further compare the adsorption and catalytic effect of catalyst on MO, ACF and ACF-nZVI after reacting with Cr(VI) solution were used for adsorption experiments. The experimental conditions were the same as those for catalytic wet oxidation of MO, i.e., temperature of 70 °C, EBCT of 1.256 min, pH 2, and inlet concentration of 50 mg/L. The breakthrough curve and adsorption rate are shown in Figure 9. It can be seen from Figure 9 that MO could be adsorbed by unused ACF and the breakthrough concentration of MO was lower than 0.05 in 340 min. The breakthrough concentration of MO reached 0.073, i.e., the adsorption ratio of MO was 92.7% at 360 min. After that, the adsorption rate of MO decreased rapidly and the adsorption ratio was only 4.9% at 480 min. The ACF-nZVI after reacting with Cr(VI) solution had little adsorption effect on MO and the concentration of outlet solution was basically the same as that of inlet solution. However, when ACF-nZVI, after reacting with Cr(VI) solution, was reused for CWPO of MO three times, i.e., 720 min continuously, the conversion ratio of MO remained 99.2%. The conversion ratio of MO remained largely unchanged within the experimental period.

CONCLUSIONS

In this study, the application of ACF-nZVI for the continuous removal of Cr(VI) and MO from aqueous solution was fully investigated. The results are as follows:

(1) ACF-nZVI has a better performance for Cr(VI) removal compared with the ACF alone in a fixed bed. The breakthrough concentration reached 6.9% of the inlet concentration at 150 min for ACF, and the breakthrough concentration reached 5.5% at 250 min for ACF-nZVI. The removal of Cr(VI) in the fixed bed was highly dependent on the pH, bed height and inlet concentration. The breakthrough time decreased with the decrease of bed height but increased with the decrease of pH and inlet concentration.
(2) The Yoon–Nelson model was found to fit well with the experimental results. The rate constant (k_{YN}) values increased with increasing inlet concentration. The 50% breakthrough time (τ) increased with decreasing pH or

Downloaded from http://iwaponline.com/wst/article-pdf/82/4/732/744832/wst082040732.pdf
by guest

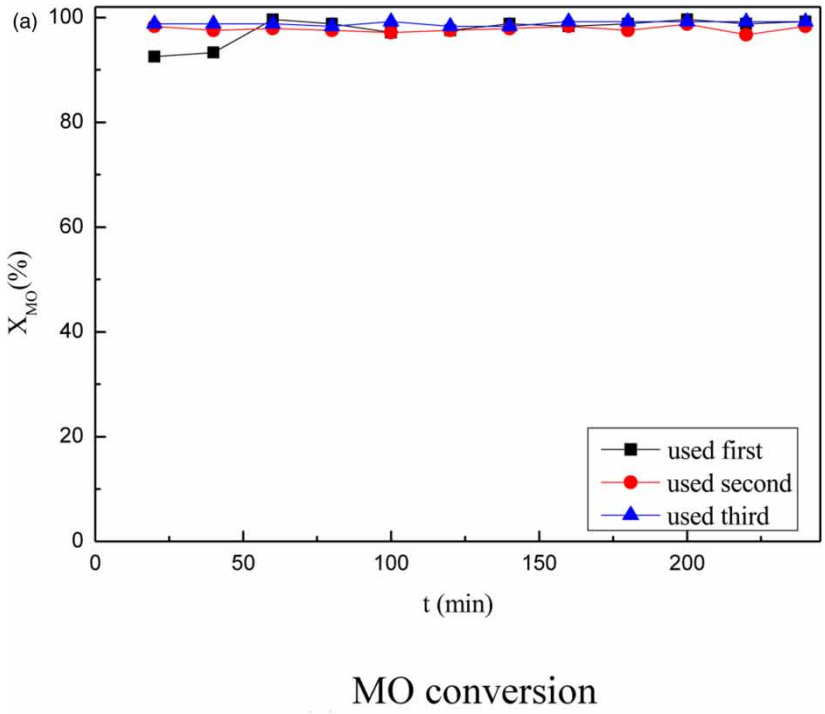

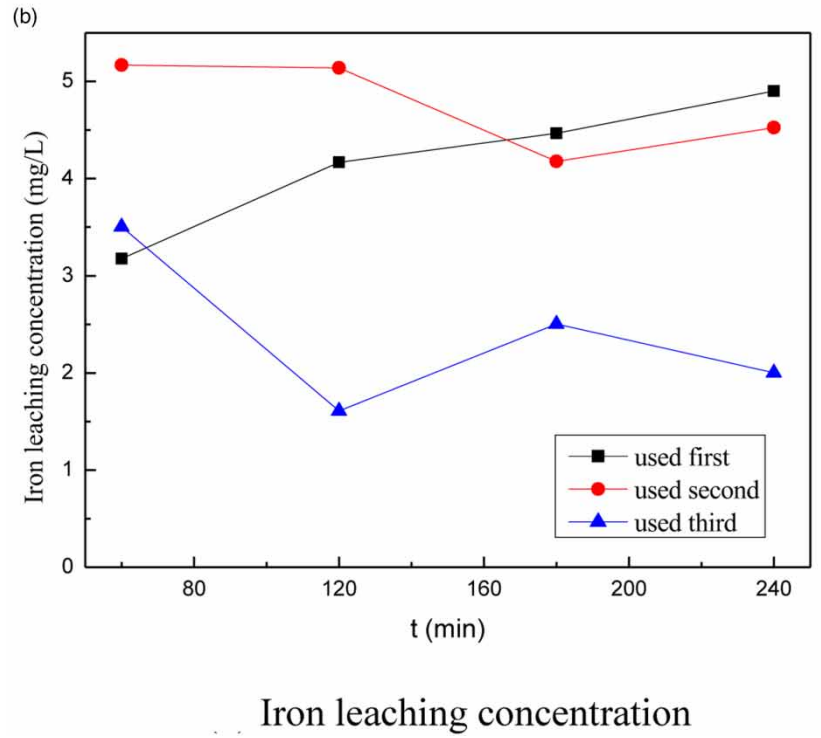

Figure 8 | Stability test.

inlet concentration, but decreased with decreasing bed height. The τ values fitted by the Yoon–Nelson model were close to the experimental data.

(3) The BDST model could predict the breakthrough time and adsorption capacity (N_0). The adsorption capacity of the ACF-nZVI was two times higher than that of

Downloaded from http://iwaponline.com/wst/article-pdf/82/4/732/744832/wst082040732.pdf
by guest

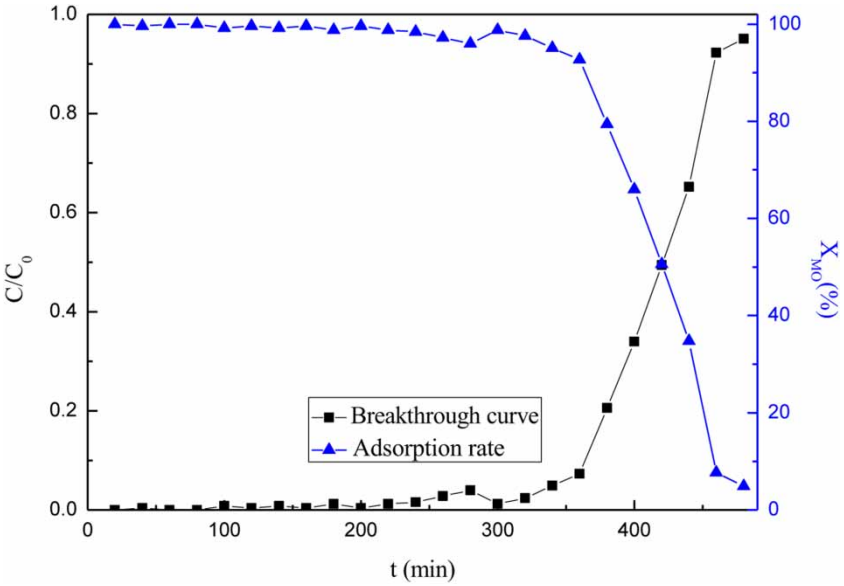

Figure 9 | Breakthrough curve and adsorption rate of MO using ACF as an adsorbent.

ACF. The values of N_0 increased with the decrease of pH and initial Cr(VI) concentration but decreased with the decrease of bed height.

(4) With the decrease of EBCT from 2.512 to 0.628 min, the conversion ratio of MO remained unchanged at first and then decreased sharply. After three successive runs (namely 720 min), the fixed bed with ACF-nZVI still retained high MO conversion (99.2%), but the adsorption ratio was only 4.9% at 480 min for ACF alone.

(5) Compared with the batch reactor, the continuous fixed bed reactor saves the non-reactive time such as feeding and unloading. However, the high flow rate leads to the short contact time between the ACF-nZVI and Cr(VI)/MO, which causes the low utilization rate of ACF-nZVI. How to improve the reaction efficiency of ACF-nZVI and increase the Cr(VI)/MO removal capacity requires future research.

ACKNOWLEDGEMENT

This work was supported by the National Natural Science Foundation of China (No. 41773133), Scientific Research Fund of Hunan Provincial Education Department, China (No. 17A028), Natural Science Foundation of Hunan Province, China (No. 2019JJ50013), and the Science and Technology Development Project of Hengyang City, China (No. 2019yj011171).

DATA AVAILABILITY STATEMENT

All relevant data are included in the paper or its Supplementary Information.

REFERENCES

Afroze, S. & Sen, T. K. 2016 Adsorption performance of continuous fixed bed column for the removal of methylene blue (MB) dye using *Eucalyptus sheathiana* bark biomass. *Research on Chemical Intermediates* **42**, 2343–2364.

Albayati, T. M., Sabri, A. A. & Alazawi, R. A. 2016 Separation of Methylene Blue as pollutant of water by SBA-15 in a fixed-bed column. *Arabian Journal for Science and Engineering* **41**, 2409–2415.

Basu, M., Guha, A. K. & Ray, L. 2019 Adsorption of lead on lentil husk in fixed bed column bioreactor. *Bioresource Technology* **283**, 86–95.

Carraro, P. S., Spessato, L., Crespo, L. H. S., Yokoyama, J. T. C., Fonseca, J. M., Bedin, K. C., Ronix, A., Cazetta, A. L., Silva, T. L. & Almeida, V. C. 2019 Activated carbon fibers prepared from cellulose and polyester-derived residues and their application on removal of Pb^{2+} ions from aqueous solution. *Journal of Molecular Liquids* **289**, 111150.

Chatterjee, S., Mondal, S. & De, S. 2018 Design and scaling up of fixed bed adsorption columns for lead removal by treated laterite. *Journal of Cleaner Production* **177**, 760–774.

Chen, S. H., Yue, Q. Y., Gao, B. Y., Li, Q., Xu, X. & Fu, K. F. 2012 Adsorption of hexavalent chromium from aqueous solution by modified corn stalk: a fixed-bed column study. *Bioresource Technology* **113**, 114–120.

Downloaded from http://iwaponline.com/wst/article-pdf/82/4/732/744832/wst082040732.pdf
by guest

Chen, H. C., Qu, X. L., Liu, N., Wang, S. F., Chen, X. L. & Liu, S. J. 2018 Study of the adsorption process of heavy metals cations on kraft lignin. *Chemical Engineering Research & Design* **139**, 248–258.

Cui, Z. H., Fang, H. W., Huang, L., Ni, K. & Reible, D. 2017 Effect of surface heterogeneity on phosphorus adsorption onto mineral particles: experiments and modeling. *Journal of Soils and Sediments* **17**, 2887–2898.

Dai, Y., Hu, Y. C., Jiang, B. J., Zou, J. L., Tian, G. H. & Fu, H. G. 2016 Carbothermal synthesis of ordered mesoporous carbon-supported nano zero-valent iron with enhanced stability and activity for hexavalent chromium reduction. *Journal of Hazardous Materials* **309**, 249–258.

Diao, Z. H., Xu, X. R., Chen, H., Jiang, D., Yang, Y. X., Kong, L. J., Sun, Y. X., Hu, Y. X., Hao, Q. W. & Liu, L. 2016 Simultaneous removal of Cr(VI) and phenol by persulfate activated with bentonite-supported nanoscale zero-valent iron: reactivity and mechanism. *Journal of Hazardous Materials* **316**, 186–193.

Dissanayake, D. M. R. E. A., Chathuranga, P. K. D., Perera, P. I., Vithanage, M. & Iqbal, M. C. M. 2016 Modeling of Pb(II) adsorption by a fixed-bed column. *Bioremediation Journal* **20**, 194–208.

Dong, H. R., Zeng, Y. L., Zeng, G. M., Huang, D. L., Liang, J., Zhao, F., He, Q., Xie, Y. K. & Wu, Y. N. 2016 EDDS-assisted reduction of Cr(VI) by nanoscale zero-valent iron. *Separation and Purification Technology* **165**, 86–91.

Dong, H. R., Den, J. M., Xie, Y. K., Zhang, C., Jiang, Z., Cheng, Y. J., Hou, K. J. & Zeng, G. M. 2017 Stabilization of nanoscale zero-valent iron (nZVI) with modified biochar for Cr(VI) removal from aqueous solution. *Journal of Hazardous Materials* **332**, 79–86.

Du, Z. L., Zheng, T. & Wang, P. 2018 Experimental and modelling studies on fixed bed adsorption for Cu(II) removal from aqueous solution by carboxyl modified jute fiber. *Powder Technology* **338**, 952–959.

Fan, Z. X., Zhang, Q., Gao, B., Li, M., Liu, C. Y. & Qiu, Y. 2019 Removal of hexavalent chromium by biochar supported nZVI composite: batch and fixed-bed column evaluations, mechanisms, and secondary contamination prevention. *Chemosphere* **217**, 85–94.

Fang, H. W., Cui, Z. H., He, G. J., Huang, L. & Chen, M. H. 2017 Phosphorus adsorption onto clay minerals and iron oxide with consideration of heterogeneous particle morphology. *Science of Total Environment* **605–606**, 357–367.

Fu, F. L., Ma, J., Xie, L. P., Tang, B., Han, W. J. & Lin, S. Y. 2013 Chromium removal using resin supported nanoscale zero-valent iron. *Journal of Environmental Management* **128**, 822–827.

Fu, R. B., Yang, Y. P., Xu, Z., Zhang, X., Guo, X. P. & Bi, D. S. 2015 The removal of chromium (VI) and lead (II) from groundwater using sepiolite-supported nanoscale zero-valent iron (S-NZVI). *Chemosphere* **138**, 726–734.

GB7467-87 1987 Water Quality – Determination of Chromium (VI) – 1, 5-Diphenylcarbohydrazide Spectrophotometric Method. National Standards of the People's Republic of China.

GB11914-89 1989 Water Quality – Determination of Chemical Oxygen Demand – Dichromate Method. National Standards of the People's Republic of China.

Ghosh, P. K. 2009 Hexavalent chromium [Cr(VI)] removal by acid modified waste activated carbons. *Journal of Hazardous Materials* **171**, 116–122.

Herney-Ramireza, J., Silva, A. M. T., Vicented, M. A., Costa, C. A. & Madeira, L. 2011 Degradation of acid orange 7 using a saponite-based catalyst in wet hydrogen peroxide oxidation: kinetic study with the Fermi's equation. *Applied Catalysis B: Environmental* **101**, 197–205.

Huang, L. H., Zhou, S. J., Jin, F., Huang, J. & Bao, N. 2014 Characterization and mechanism analysis of activated carbon fiber felt-stabilized nanoscale zero-valent iron for the removal of Cr(VI) from aqueous solution. *Colloids and Surfaces A: Physicochemical and Engineering Aspects* **447**, 59–66.

Hutchins, R. A. 1973 New method simplifies design of activated carbon systems. *Chemical Engineering* **80**, 133–135.

Kim, J. H., Kim, J. H., Bokare, V., Kim, E. J., Chang, Y. Y. & Chang, Y. S. 2012 Enhanced removal of chromate from aqueous solution by sequential adsorption–reduction on mesoporous iron–iron oxide nanocomposites. *Journal of Nanoparticle Research* **14**, 1010–1021.

Li, X. C., Huang, L., Fang, H. W., He, G. J., Reible, D. & Wang, C. H. 2019 Immobilization of phosphorus in sediments by nano zero-valent iron (nZVI) from the view of mineral composition. *Science of the Total Environment* **694**, 133695.

Liu, F. L., Yang, J. H., Zuo, J. N., Ma, D., Gan, L. L., Xie, B. M., Wang, P. & Yang, B. 2014 Graphene-supported nanoscale zero-valent iron: removal of phosphorus from aqueous solution and mechanistic study. *Journal of Environmental Sciences* **26**, 1751–1762.

Liu, Q. X., Zhou, Y. R., Wang, M., Zhang, Q., Ji, T., Chen, T. Y. & Yu, D. C. 2019 Adsorption of methylene blue from aqueous solution onto viscose-based activated carbon fiber felts: kinetics and equilibrium studies. *Adsorption Science & Technology* **37**, 312–332.

Luca, C. D., Massa, P., Grau, J. M., Marchetti, S. G., Fenoglio, R. & Haure, P. 2018 Highly dispersed Fe^{3+}-Al_2O_3 for the Fenton-like oxidation of phenol in a continuous up-flow fixed bed reactor. Enhancing catalyst stability through operating conditions. *Applied Catalysis B: Environmental* **237**, 1110–1123.

Martínez-Huitle, C. A. & Brillas, E. 2009 Decontamination of wastewaters containing synthetic organic dyes by electrochemical methods: a general review. *Applied Catalysis B: Environmental* **87**, 105–145.

Mishra, A., Tripathi, B. D. & Rai, A. K. 2016 Packed-bed column biosorption of chromium(VI) and nickel(II) onto Fenton modified *Hydrilla verticillata* dried biomass. *Ecotoxicology and Environmental Safety* **132**, 420–428.

Mohamed, A., Osman, T. A., Toprak, M. S., Muhammed, M., Yilmaz, E. & Uheida, A. 2016 Visible light photocatalytic reduction of Cr(VI) by surface modified CNT /titanium dioxide composites nanofibers. *Journal of Molecular Catalysis A: Chemical* **424**, 45–53.

Neamţu, M., Zaharia, C., Catrinescu, C., Yediler, A., Macoveanu, M. & Kettrup, A. 2004 Fe-exchanged Y zeolite as catalyst for

Downloaded from http://iwaponline.com/wst/article-pdf/82/4/732/744832/wst082040732.pdf
by guest

wet peroxide oxidation of reactive azo dye Procion Marine H-EXL. *Applied Catalysis B: Environmental* **48**, 287–294.

Nethaji, S. & Sivasamy, A. 2014 Removal of hexavalent chromium from aqueous solution using activated carbon prepared from walnut shell biomass through alkali impregnation processes. *Clean Technologies and Environmental Policy* **16**, 361–368.

Qu, G. Z., Kou, L. Q., Wang, T. C., Liang, D. L. & Hu, S. B. 2017 Evaluation of activated carbon fiber supported nanoscale zero-valent iron for chromium (VI) removal from groundwater in a permeable reactive column. *Journal of Environmental Management* **201**, 378–387.

Quintanilla, A., Fraile, A. F., Casas, J. A. & Rodríguez, J. J. 2007 Phenol oxidation by a sequential CWPO-CWAO treatment with a Fe/AC catalyst. *Journal of Hazardous Materials* **146**, 582–588.

Ramirez, J. H., Maldonado-Hódar, F. J., Pérez-Cadenas, A. F., Moreno-Castilla, C., Costa, C. A. & Madeira, L. M. 2007 Azo-dye Orange II degradation by heterogeneous Fenton-like reaction using carbon-Fe catalysts. *Applied Catalysis B: Environmental* **75**, 312–323.

Rangabhashiyam, S. & Selvaraju, N. 2015 Adsorptive remediation of hexavalent chromium from synthetic wastewater by a natural and $ZnCl_2$ activated *Sterculia guttata* shell. *Journal of Molecular Liquids* **207**, 39–49.

Sakir, M. & Onses, M. S. 2019 Solid substrates decorated with Ag nanostructures for the catalytic degradation of methyl orange. *Results in Physics* **12**, 1133–1141.

Shang, T. X., Zhang, J., Jin, X. J. & Gao, J. M. 2014 Study of Cr(VI) adsorption onto nitrogen-containing activated carbon preparation from bamboo processing residues. *Journal of Wood Science* **60**, 215–224.

Sheng, G. D., Hu, J., Li, H., Li, J. X. & Huang, Y. Y. 2016 Enhanced sequestration of Cr(VI) by nanoscale zero-valent iron supported on layered double hydroxide by batch and XAFS study. *Chemosphere* **148**, 227–232.

Shi, L. N., Zhang, X. & Chen, Z. L. 2011 Removal of chromium(VI) from wastewater using bentonite-supported nanoscale zero-valent iron. *Water Research* **45**, 886–892.

Subbaiah, M. V. & Kim, D. S. 2016 Adsorption of methyl orange from aqueous solution by aminated pumpkin seed powder: kinetics, isotherms, and thermodynamic studies. *Ecotoxicology and Environmental Safety* **128**, 109–117.

Sun, Y. P., Li X, Q., Cao, J., Zhang, W. X. & Wang, H. P. 2006 Characterization of zero-valent iron nanoparticles. *Advances in Colloid and Interface Science* **120**, 47–56.

Vilvanathan, S. & Shanthakumar, S. 2017 Modeling of fixed-bed column studies for removal of cobalt ions from aqueous solution using *Chrysanthemum indicum*. *Research on Chemical Intermediates* **43**, 229–243.

Wang, Y., Gao, Y. W., Chen, L. & Zhang, H. 2015 Goethite as an efficient heterogeneous Fenton catalyst for the degradation of methyl orange. *Catalysis Today* **252**, 107–112.

Wu, L. M., Liao, L. B., Lv, G. C., Qin, F. X., He, Y. J. & Wang, X. Y. 2013 Micro-electrolysis of Cr (VI) in the nanoscale zero-valent iron loaded activated carbon. *Journal of Hazardous Materials* **254–255**, 277–283.

Xu, C. H., Zhu, L. J., Wang, X. H., Lin, S. & Chen, Y. M. 2014 Fast and highly efficient removal of chromate from aqueous solution using nanoscale zero-valent iron/activated carbon (NZVI/AC). *Water Air and Soil Pollution* **225**, 1845–1857.

Yan, Y., Jiang, S. S. & Zhang, H. P. 2014 Efficient catalytic wet peroxide oxidation of phenol over Fe-ZSM-5 catalyst in a fixed bed reactor. *Separation and Purification Technology* **133**, 365–374.

Yan, J., Zhu, Y., Qiu, F. X., Zhao, H., Yang, D. Y., Wang, J. & Wen, W. Y. 2016 Kinetic, isotherm and thermodynamic studies for removal of methyl orange using a novel β-cyclodextrin functionalized graphene oxide-isophorone diisocyanate composites. *Chemical Engineering Research & Design* **106**, 168–177.

Zhang, X., Lin, S., Lu, X. Q. & Chen, Z. L. 2010 Removal of Pb(II) from water using synthesized kaolin supported nanoscale zero-valent iron. *Chemical Engineering Journal* **163**, 243–248.

Zhang, X., Lin, S., Chen, Z. L., Meghara, M. & Naidu, R. 2011 Kaolinite-supported nanoscale zero-valent iron for removal of Pb^{2+} from aqueous solution: reactivity, characterization and mechanism. *Water Research* **45**, 3481–3488.

Zhang, J., Zhang, W. & Zhang, Y. 2015 Pore structure characteristics of activated carbon fibers derived from poplar bark liquefaction and their use for adsorption of Cu(II). *BioResources* **10**, 566–574.

Zhang, D. S., Gao, W. Q., Chang, G. Z., Luo, S., Jiao, W. Z. & Liu, Y. Z. 2019 Removal of heavy metal lead(II) using nanoscale zero-valent iron with different preservation methods. *Advanced Powder Technology* **30**, 581–589.

Zhou, X. B., Lv, B. H., Zhou, Z. M., Li, W. X. & Jing, G. H. 2015 Evaluation of highly active nanoscale zero-valent iron coupled with ultrasound for chromium(VI) removal. *Chemical Engineering Journal* **281**, 155–163.

First received 15 March 2020; accepted in revised form 28 July 2020. Available online 12 August 2020

Downloaded from http://iwaponline.com/wst/article-pdf/82/4/732/744832/wst082040732.pdf
by guest